ESMO Open Cancer Horizons

Brain microenvironment-driven resistance to immune and targeted therapies in acral melanoma

Rebecca Jane Lee ,[1] Garima Khandelwal,[2] Franziska Baenke,[1,3] Alessio Cannistraci,[1] Kenneth Macleod,[4] Piyushkumar Mundra,[1] Garry Ashton,[5] Amit Mandal,[1] Amaya Viros,[1,6] Gabriela Gremel,[1,7] Elena Galvani,[1] Matthew Smith,[1] Neil Carragher,[4] Nathalie Dhomen,[1] Crispin Miller,[2] Paul Lorigan,[8,9] Richard Marais[1]

► Additional material is published online only. To view please visit the journal online (http://dx.doi.org/10.1136/esmoopen-2020-000707).

To cite: Lee RJ, Khandelwal G, Baenke F, *et al*. Brain microenvironment-driven resistance to immune and targeted therapies in acral melanoma. *ESMO Open* 2020;**5**:e000707. doi:10.1136/esmoopen-2020-000707

Received 11 February 2020
Revised 30 April 2020
Accepted 2 May 2020

For numbered affiliations see end of article.

Correspondence to
Dr Richard Marais;
Richard.Marais@cruk.manchester.ac.uk

ABSTRACT

Background Combination treatments targeting the MEK-ERK pathway and checkpoint inhibitors have improved overall survival in melanoma. Resistance to treatment especially in the brain remains challenging, and rare disease subtypes such as acral melanoma are not typically included in trials. Here we present analyses from longitudinal sampling of a patient with metastatic acral melanoma that became resistant to successive immune and targeted therapies.

Methods We performed whole-exome sequencing and RNA sequencing on an acral melanoma that progressed on successive immune (nivolumab) and targeted (dabrafenib) therapy in the brain to identify resistance mechanisms. In addition, we performed growth inhibition assays, reverse phase protein arrays and immunoblotting on patient-derived cell lines using dabrafenib in the presence or absence of cerebrospinal fluid (CSF) in vitro. Patient-derived xenografts were also developed to analyse response to dabrafenib.

Results Immune escape following checkpoint blockade was not due to loss of tumour cell recognition by the immune system or low neoantigen burden, but was associated with distinct changes in the microenvironment. Similarly, resistance to targeted therapy was not associated with acquired mutations but upregulation of the AKT/phospho-inositide 3-kinase pathway in the presence of CSF.

Conclusion Heterogeneous tumour interactions within the brain microenvironment enable progression on immune and targeted therapies and should be targeted in salvage treatments.

Key questions

What is already known about this subject?

- Cutaneous melanoma brain metastases have been shown to respond to both immune and targeted therapies, however response and resistance in acral melanoma remains poorly characterised.
- The phospho-inositide 3-kinase (PI3K) pathway has been shown to be important in the brain, however its influence on response to treatment has not previously been tested using patient-derived models of melanoma and specifically acral melanoma brain metastases.

What does this study add?

- Despite low neoantigen burden, patients with acral melanoma can derive benefit from immune therapy. Immune therapy escape in the brain was not associated with mutational changes, however there was decreased infiltration of effector T cells, an increase in alternatively activated macrophages and distinct changes in gene expression, suggesting the brain microenvironment enabled immune escape. In addition, testing of patient-derived xenografts and cell lines showed that resistance to targeted therapy in the brain was mediated by extrinsic factors resulting in activation of the PI3K/AKT pathway.

How might this impact on clinical practice?

- The PI3K/AKT pathway is an important target for melanoma brain metastases. Precision medicine must address the interactions of the tumour with the brain microenvironment and tailor therapies according to the site of progression in addition to its genomic features.

INTRODUCTION

The treatment landscape of melanoma has changed dramatically in recent years. With the advent of combination treatments targeting the MEK-ERK pathway and the parallel development of immune checkpoint inhibitors, patients can now expect to survive a median of 36 months with a proportion achieving durable remissions.[1] Despite these impressive advances, most patients treated with these agents still progress and die from their disease, and brain metastasis in particular remains a persistent clinical challenge.[2 3] Recent studies have shown that although response to targeted and immune therapies can be obtained in melanoma brain metastases, duration of response is shorter than for patients with extracranial disease alone.[2 4] Understanding of mechanisms of resistance is therefore crucial.

Notably, the majority of clinical trials involve patients with common cutaneous melanoma and only a small number of patients with acral melanoma have been included.[5] Interrogation of the response of acral melanoma to immune and targeted therapies is an important aim. Acral melanoma is a rare cutaneous melanoma subtype found on non-hair bearing skin such as the palms, nail beds and soles,[6] and accounts for 2%–3% of melanomas.[7] The genetic alterations in acral melanoma are distinct from those in cutaneous melanoma, with *KIT* mutations more common (15%–20% vs 1%–2%) and *BRAF* mutations less common (15% vs 45%).[8 9] Furthermore, acral melanoma is associated with a lower mutational burden and higher copy number variation than common cutaneous melanoma.[8]

We show here that metastatic acral melanoma responds to both immune and targeted therapies but, as often seen with common cutaneous melanoma, resistance develops to both modalities. Through longitudinal sampling of an exceptional case of a patient with acral melanoma who had isolated progressions in the brain while responding in all other sites, first to immune and then to targeted therapy, we provide insight into the heterogeneity of the tumour microenvironment resulting in resistance to standard melanoma treatments. Improved understanding of tumour-microenvironment interactions will provide hypothesis-driven salvage therapies that target the drivers of tumourigenesis, and the distinct tumour microenvironments.

METHODS

RNA/DNA extraction

Following microdissection of the tumour to ensure tumour purity, RNA/DNA was extracted using the AllPrep DNA/RNA Micro Kit (Qiagen) according to manufacturer's instructions. Whole-exome sequencing (WES) and RNA-Seq were performed as previously described.[10 11]

RNA-Seq analysis

The RNA-Seq data were aligned to human GRCh37 assembly by MapSplice (V.2.1.6)[12] and further analysis performed in R (V.3.1.0). Gene counts were extracted using featureCounts[13] for Ensembl V.73 annotation (V.1.16.1), which were then converted into reads per kilobase million (RPKM). The RPKM values are used for all expression-level quantification of the genes. Genes overexpressed in the brain lesion ($\log_2$FC≥2) as compared with the baseline lesion were used to perform over-representation analysis using the gProfileR package (V.0.5.3).[14] From the over-representation analysis on gene ontology, we represented biological processes in a network using Cytoscape.[15]

WES analysis

WES data were aligned to human GRCh37 with bwa-mem (V.0.7.7).[16] Deduplication, realignment and recalibration was performed on the aligned data as suggested in the Genome Analysis Toolkit (GATK) framework.[17] Somatic mutation calling was then done using MuTect (V.1.1.7).[18]

Neoantigen determination

Non-synonymous mutations were scanned and candidate nonamer peptides identified. The human leukocyte antigen (HLA) type of the patient was determined by Central Manchester University Hospital (laboratory reference no 03 GB-009.991) to be HLA A 02:01. Candidate sequences were input into NetCTLpan V.1.1 previously validated by other groups.[19]

Droplet digital PCR

Each negative control or cell line sample was run over three replicate wells. Per well, 10 ng input DNA was added to 11 µl ddPCR Supermix for probes (no Uridine-5'-triphosphate (UTP)) (Bio-Rad) and 0.55 µl of custom designed probe (Lifetech) for phospho-inositide 3-kinase (PI3K) L25S made up to a total volume of 22 µl with water. Droplets were generated using a QX200 automated droplet generator (Bio-Rad) and a PCR reaction was performed using the following cycling conditions: 95°C for 10 min; 40 cycles of 94°C for 30 s and 55°C for 1 min; followed by 98°C for 10 min (all at a ramp rate of 2°C/s), and a final hold at 4°C (ramp rate 1°C/s). Droplets were read using a QX200 droplet reader (Bio-Rad) and the data analysed using QuantaSoft software V.1.4.0.99 (Bio-Rad).

CIBERSORT analysis

The leucocyte signature matrix LM22 (547 genes) that differentiates 22 types of tumour-infiltrating immune cells was used for the analysis. Normalised gene expression data from RNA-Seq analysis of each sample (subcutaneous and brain lesions) were processed with the Cell type Identification By Estimating Relative Subsets Of known RNA Transcripts (CIBERSORT) web tool (http://cibersort.stanford.edu/) using default parameters at 100 permutations.

Cell culture

Cell lines from patient samples were established from fresh tumour biopsies, cultured under standard conditions and were routinely monitored for mycoplasma contamination by PCR. Cells were cultured in Roswell Park Memorial Institute (cell culture media) (RPMI) supplemented with 10% fetal bovine serum (FBS) and 1% penicillin/streptomycin.

Short-term growth inhibition assays

Cultured cells from the subcutaneous and brain metastases were seeded into 96-well plates (3000 cells per well). Twenty-four hours later, serial dilutions of dabrafenib (Selleckchem) were added. Cells were incubated for a further 72 hours and viability measured by CellTiter-Glo assays (Promega). Relative survival in the presence of drugs was normalised to the untreated controls after background subtraction. Data from one representative experiment are shown.

Quantification of cell death

Rat cerebrospinal fluid (CSF) was collected as previously described.[20] Cells were cultured overnight in RPMI or 50% CSF, treated with dimethyl sulfoxide (DMSO) or dabrafenib (1 µM) for 24 hours, then fixed with methanol. Cell death was assessed through blocking with 0.5% bovine serum albumin for 1 hour then incubating with 0.3% cleaved poly (ADP-ribose) polymerase (PARP) conjugated with alexa fluor 647 (#6987 Cell Signaling Technology) in 0.5% bovine serum albumin for 1 hour and acquiring stained cells on an LSR II flow cytometer (BD Biosciences). Data of duplicate experiments were analysed using FlowJo software V.10.0.8.

Twenty-four hours growth inhibition assay in the presence of CSF

Cells were cultured overnight under serum-free conditions in RPMI or 50% rat CSF and then treated with DMSO, dabrafenib (1 µM), BEZ235 (5 µM) or dabrafenib (1 µM) plus BEZ235 (5 µM) (Selleckchem) for 24 hours, at which point viability was measured by CellTiter-Glo assays (Promega). Relative survival was normalised to DMSO controls in either media or in the presence of CSF. Data from one representative experiment is shown.

Statistical analyses

Unpaired, two-tailed T tests were performed using GraphPad Prism software V.7.0a and Microsoft Excel V.14.6.9.

Histology and immunohistochemistry

Tumours were formalin-fixed and stained with H&E and anti-major histocompatibility complex (MHC) class I+HLA A+HLA B antibody (EPR1394Y) (Abcam).

Multiplexing and quantification of immune infiltrate

From each formalin-fixed, paraffin-embedded block, 5 µm sections were stained with anti-CD4 (MABF750 0.3 µg/mL), anti-CD8 (M7103 2 µg/mL), anti-CD-163 (NCL-CD163 5 µg/mL) and HMB45 (ab732 2 µg/mL). Immunohistochemistry (IHC) was performed on a Ventana Discovery Ultra platform. Following deparaffinisation and blocking of endogenous peroxidase the antibodies were applied sequentially in the order listed. Following heat-induced epitope retrieval using cell conditioning two (32 mins at 95°) omnimap antimouse horseradish peroxidase (HRP) (760–4310) or omnimap antirabbit HRP (760–4311) were used to detect the primaries. Following HRP labelling, a Perkin Elmer Opal plex kit was used (NEL791001KT). CD4 was labelled with Cy5.5, CD8 with fluorescein isothiocyanate (FITC) and HMB45 (Cy3). A heat step of 8 min (using CC2 at 95°) was applied after each label.

Multiplexed tissue (bright-field and fluorescence) was visualised at ×400 total magnification and ×20 image fields were acquired. Vectra V.2.0 and Nuance V.2.0 software packages (Perkin Elmer, Waltham, Massachusetts, USA) were used for automated image acquisition and development of the spectral library, respectively. Vectra multispectral image files were then converted into multilayer Tagged Image File Format (TIFF) format using inForm (PerkinElmer, Waltham, Massachusetts) and a customised spectral library created. These were converted to single layer TIFF files using ImageJ (Fiji). Tumour/stroma identification and marker quantification were performed using Definiens Developer XD (Definiens AG, Munich, Germany) and Definiens tissue studio (Definiens AG, Munich, Germany).

Cell lysates and immunoblots

Cells were cultured overnight under serum-free conditions in RPMI or 50% rat CSF and then treated with DMSO or dabrafenib (1 µM) for 4 hours. Cell lysates were prepared with Nonidet™ P40 (NP40) buffer containing 5% ß-mercaptoethanol, 150 mM NaCl, 50 mM Tris pH 7.5, 2 mM EDTA pH 8, 25 mM sodium fluoride (NaF) and 1% NP40, protease inhibitors (Complete, Roche), phosphatase inhibitor cocktails II and III (Sigma). All lysates were freshly prepared and resolved by SDS gel electrophoresis for western blotting. Primary antibodies were: p44/42 mitogen-activated protein kinase (MAPK) (Erk1/2) (137F5) (Cell Signaling Technology) p-ERK1/2 (MAPK-YT) (Sigma Aldrich), AKT1 (2H10), phosphoprotein kinase B (pAKT) (S473) and pAKT (T308, 244F9) (Cell Signaling Technology). Specific bands were detected using fluorescent-labelled secondary antibodies (Invitrogen; LI-COR Biosciences) and analysed using an Odyssey infrared scanner (LI-COR Biosciences). Immunoblots were performed in duplicate.

Reverse phase protein array

Cells were cultured overnight under serum-free conditions in RPMI or 50% rat CSF and then treated with DMSO or dabrafenib (1 µM) for 4 hours. Lysates were freshly prepared and fluorescence based nitrocellulose reverse phase protein array (RPPA) was performed as previously described.[21]

Collection of patient samples

Patient samples were collected with written, fully informed patient consent under Manchester Cancer Research Centre (MCRC) Biobank ethics application #07/H1003/161+5 and approval for the work under MCRC Biobank Access Committee application 13_RIMA_01.

Animal procedures

All procedures involving animals were performed in accordance with National Home Office regulations under the Animals (Scientific Procedures) Act 1986 and within guidelines set out by the Cancer Research UK, MI Manchester Institute (CRUK MI's) Animal Welfare and Ethical Review Board, carried out under license PPLPE3DF1A5B (formerly PPL70/7701), and reported in accordance with ARRIVE guidelines. Mice were maintained in pathogen-free, ventilated cages in the Biological Resources Unit at CRUK MI with free access to irradiated food and autoclaved water in a 12-hour light/dark cycle,

with room temperature at 21±2°C. Cages contained wood shavings, bedding and a cardboard tube. All procedures were conducted in the light phase.

Establishing and dosing of patient-derived xenografts

Patient tumour samples (~80 mm^3) were implanted subcutaneously in flanks of 6-week-old female NOD scid gamma (NSG) mice. These were expanded in a further passage of mice and experiments performed in passage 3. Animals were dosed by daily orogastric gavage with dabrafenib (Selleckchem) 25 mg/kg or vehicle (5% DMSO in water). For the subcutaneous lesion, 14 animals were randomised when tumours were between 50 mm^3 and 120 mm^3 into groups receiving dabrafenib or vehicle for up to 40 days. For the brain lesion, 20 animals were randomised on a rolling recruitment basis when tumours reached 50–120 mm^3 into groups receiving dabrafenib or vehicle for up to 38 days. Tumour volume was determined by calliper measurements of tumour length (L), width (W) and depth (D), and calculated as volume=L×W×D×$\pi/6$, measured from the day treatment commenced until volume approached 1500 mm^3 or the mouse was euthanised for welfare reasons.

RESULTS

Neoepitope expression, IFNγ signalling and antigen processing are conserved in the brain lesion that had escaped immune-surveillance

We describe a patient in their early 40s who presented acral melanoma on the sole of the right foot (figure 1A, green lesion). The tumour was resected, but recurred at the original scar site 2 years later and was again removed. A year later, the patient developed widespread disease, with a subcutaneous lesion in the right thigh, and several metastases in the hilar lymph nodes, liver and lungs (figure 1A). To alleviate clinical symptoms, the subcutaneous thigh tumour was resected, providing a pretreatment baseline sample. The other lesions were inoperable, so nivolumab (3 mg/kg every 2 weeks) was administered and the patient achieved an excellent response for M1c disease, with disappearance of all of the tumours in the hilum, liver and lung. These tumours did not return, but despite this remarkable ongoing systemic response, an isolated lesion in a mediastinal lymph node slowly progressed and 7 months after starting nivolumab was confirmed to be PET-positive. This immune-refractory lesion was resected, and imaging confirmed the patient was disease-free and continued to respond to nivolumab. Unfortunately, despite the excellent ongoing response, after 12 months the patient developed grade 3 diarrhoea, necessitating nivolumab withdrawal. Within a month, the patient presented with neurological symptoms at another hospital and MRI scan revealed a new solitary metastasis in the brain that was resected (figure 1A).

The thigh resection provided a baseline pretreatment tumour from a patient who presented a complete response to nivolumab, and the brain lesion provided a tumour that had escaped the immune control normally associated with complete response to checkpoint blockade.[22] Notably, MHC class I proteins remained highly expressed in the immune-escape brain tumour (figure 1B), and melanoma associated antigen gene expression was also unaltered (online supplementary fig. 1). Thus, the immune escape in this patient's brain metastasis was not mediated by changes in antigen presentation or loss of melanoma antigens.

Consistent with previous studies in acral melanoma,[8] WES revealed a very low mutation burden, with 25 non-synonymous single nucleotide variants (SNVs) in the baseline tumour and 27 in the brain metastasis (figure 1C; online supplementary table 1). Twenty-four of these SNVs were shared mutations, revealing low genomic heterogeneity (figure 1C) and only five mutations (*SACS, PHOX2B, UGT8, CLEC10A, SCL16A13*) were predicted to generate high affinity MHC class I epitopes for cytotoxic T lymphocytes (online supplementary table 2). RNA-Seq revealed that expression of these genes did not decrease in the brain lesion (figure 1D). Moreover, all five candidate neoantigens were expressed at low levels in the baseline and immune-escape tumour (<5 RPKM; figure 1D, online supplementary table 2). Thus, immune escape was unlikely to have been mediated by loss of neoantigen expression, and we did not observe mutations in *JAK2* or related genes, which drive immune therapy resistance through interferon gamma (IFNγ) signalling or mutations resulting in loss of *PTEN*, which has been shown to result in immunosuppression.[23–25]

Nivolumab resistance is associated with a distinct gene signature and immune infiltrate

To investigate underlying mechanisms, we examined gene expression in microdissected tumour samples (to ensure tumour purity) from the lesions. We used biological processes and Kyoto Encyclopedia of Genes and Genomes (KEGG) pathway analyses of RNA-Seq expression data to reveal differences between the baseline and immune-escape brain metastasis. This showed that biological processes such as cytokine-secretion, type 2 immune response and chemokine-mediated signalling were significantly upregulated in the resistant lesion (figure 1E, online supplementary figure 2, online supplementary table 3). We did not observe a signature associated with loss of PTEN as previously described (online supplementary table 4),[24 25] and neither was there evidence of increased activation of Wnt/ß-catenin and downregulation of chemokines associated with increased Wnt/ß-catenin expression leading to resistance to anti-programmed death-1 (PD-1) therapy (online supplementary table 5).[26] Although there was an increase in expression of genes associated with many inflammatory factors, there was particularly high expression in the brain metastasis of *CXCL1* and *IL10* which are involved in tumour progression, immune tolerance and infiltration of immunosuppressive cells (figure 1E).[27–29]

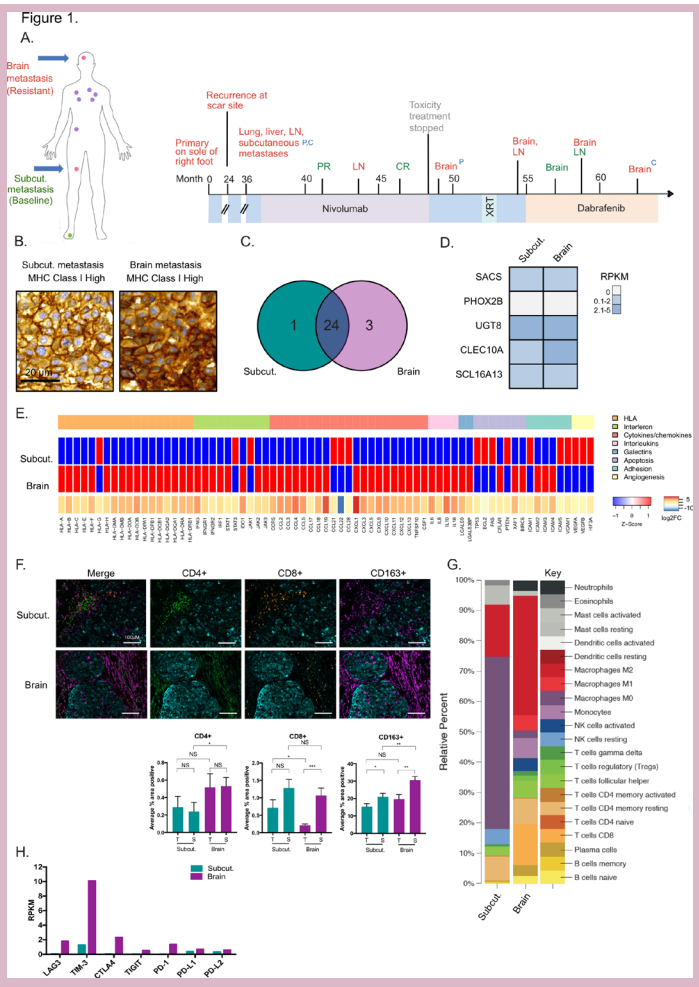

Figure 1 Immune escape in the brain is associated with a distinct microenvironment. (A) Timeline of patient's clinical history. Green font, response; red font, progressive disease; grey font, toxicity; CR, complete response; PR, partial response; P, PDX; C, cell line; XRT, whole brain radiotherapy, red lesions are areas sampled, purple lesions sites of disease spread, green lesion primary site. Subcut., subcutaneous metastasis. (B) MHC class I expression is conserved in the immune-escape lesion compared with baseline lesion. Immunohistochemistry showing MHC class I expression in the baseline and immune-escape lesions. Scale bar, 20 µM. (C) The patient's tumours have a low mutation burden. Venn diagram showing distribution of non-synonymous mutations identified by WES in the baseline (Subcut.) and immune-escape (Brain) lesions. (D) Neoantigens expression is unaltered in the baseline and immune-escape melanomas. Mutations identified through whole-exome sequencing (WES) were analysed using NetCTL and predicted neoantigens with a high affinity for MHC class I binding (score <1) are depicted. In shaded blue, the gene expression (reads per kilobase per million; RPKM) of the mutated genes present in the baseline (Subcut.) and immune-escape (Brain) lesions. (E) Nivolumab resistance is associated with upregulation of genes related to immunity. Supervised clustering of RNA-Seq data for selected genes associated with tumour-immune interaction of the baseline and immune escape brain lesion. Z-score (SD from the mean) depicted in blue, downregulated; red, upregulated. Log_2FC, log_2 fold change of the expression values (brain lesion/subcutaneous lesion) is represented in blue-yellow-red gradient. (F) Immune-escape is associated with decreased T cell infiltration. Example photomicrograph images depicting heterogeneous composition of immune cell infiltrates within tumour and stroma. Left panel is overlay of the four different markers: green, $CD4^+$; orange, $CD8^+$; purple, CD163+; cyan, HMB45. Quantification (mean and SD) for multiple panels of immune cell infiltrate in each lesion using Definiens is below each representative panel. NS, not significant; *p<0.05; **p<0.01; ***p<0.001. (G) Immune-escape is associated with heterogeneous immune cell infiltration using CIBERSORT. Bar chart summarising immune cell subset proportion of 22 types of adaptive and innate immune cells quantified by CIBERSORT for the three lesions. (H) Immune-escape is associated with altered expression of immunomodulatory genes. Gene expression of immunomodulators quantified in the baseline (Subcut.) and immune-escape (Brain) lesions based on RNA-Seq analysis.

Thus, compared with the baseline, the immune-escape tumour presented a distinct gene signature, so we examined immune cell infiltrates in these lesions by multiplex IHC. This revealed a trend towards higher CD4+ and CD163+ infiltrate in the brain metastasis in both tumour and stromal areas compared with the subcutaneous lesion (figure 1F). Critically, CD8+ infiltrate was significantly decreased in the brain lesion tumour area compared with both its surrounding stroma and also compared with the tumour area of the subcutaneous lesion (figure 1F).

We performed CIBERSORT[30] to further examine the immune cell infiltrate. This revealed that the subcutaneous

lesion had a higher presence of M0 macrophages, while the brain lesion presented a higher proportion of alternatively activated (M2) macrophages and regulatory T cells, which are immunosuppressive and have been linked to the lack of response to anti-PD-1 therapy (figure 1G).[31 32] Finally, the brain metastasis also presented mRNA upregulation of immunomodulators such as *TIM3* and *LAG3*, which are associated with T cell exhaustion,[33] and thereby tumour escape from the immune system (figure 1H). Thus, the immune-escape brain lesion was associated with a general increase in inflammation and negative immune mediators with infiltrate of cells associated with immunosuppression and decrease infiltrate of effector T cells compared with the pretreatment subcutaneous lesion.

Resistance to targeted therapy in the brain

Following resection of the brain lesion, the patient received whole brain radiation, but progressed within 3 months with regrowth of the brain tumour, and the appearance of a new paraoesophageal lymph node tumour (figure 1A). As the patient's tumour harboured a p.V600E *BRAF* mutation, dabrafenib was administered and the patient achieved resolution of the lymph node lesion and a partial response in the brain (50% decrease). Intriguingly, despite an ongoing extracranial response to dabrafenib, after 3 months the brain lesion progressed and was resected (figure 2A). The patient continued on dabrafenib, but the brain metastasis progressed after a further 4 months and was once again resected. The patient remained stable on dabrafenib until progression 2 months later, when tumour infiltrating lymphocyte (TIL) therapy was administered, but the patient passed away shortly after.

We developed a patient-derived xenograft from the pre dabrafenib brain lesion, and a cell line from the progressing brain lesion and used those to determine how dabrafenib resistance in the brain was mediated.

Figure 2.

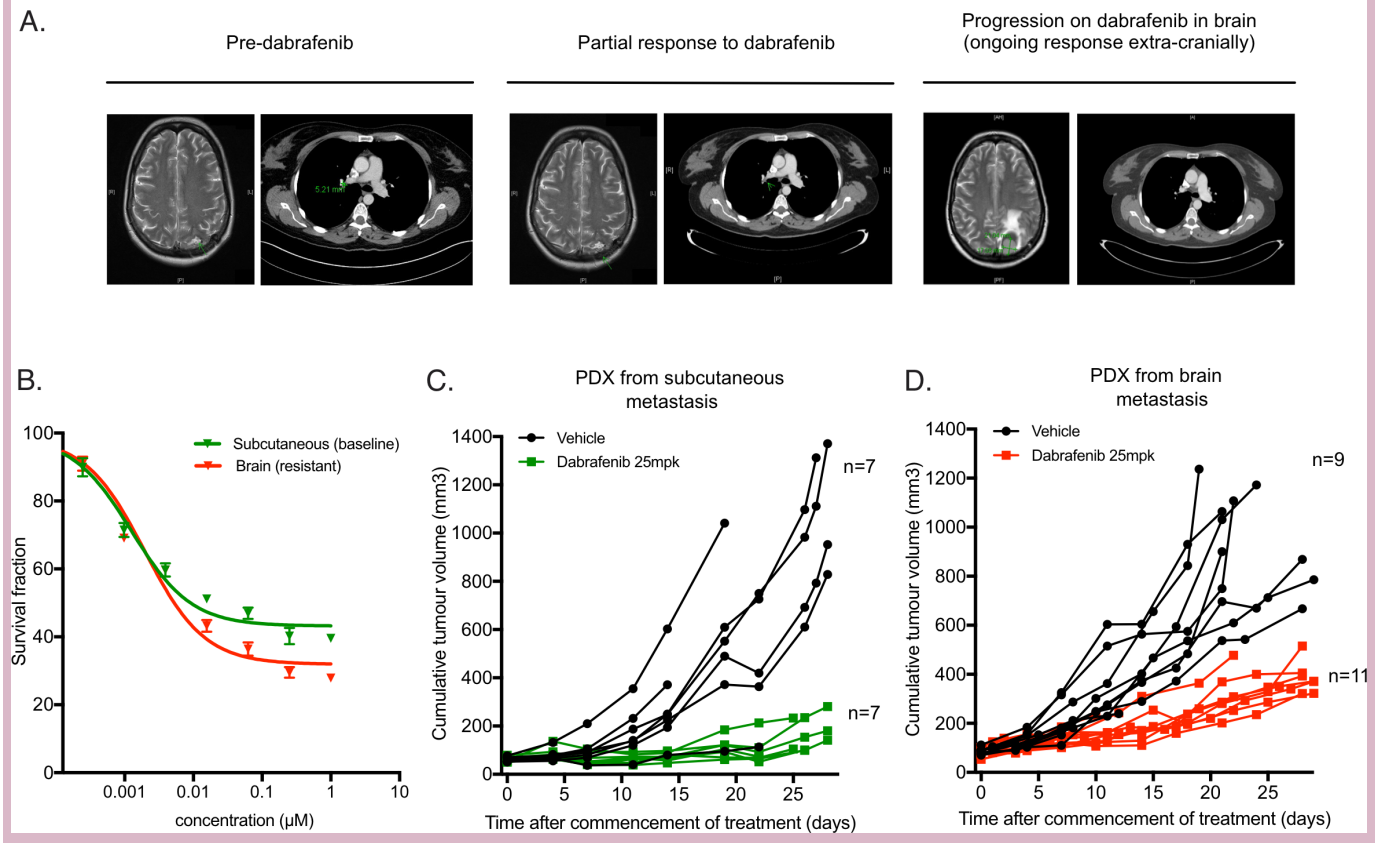

Figure 2 Brain lesions retain dabrafenib sensitivity outside the brain microenvironment. (A) CT images of patient's brain lesion and paraoesophageal lesion in response to dabrafenib. Left CT images show predabrafenib (brain lesion measuring 1×0.9 cm), middle images show partial response to dabrafenib (brain lesion measuring 0.9×0.5 cm) and right images show disease progression in the brain (brain lesion measuring 2.1×1.7 cm) and ongoing response in extracranial sites on dabrafenib. (B) Cells derived from the dabrafenib-resistant brain lesion remain sensitive to dabrafenib in vitro. Short-term growth inhibition assays (72 hours) of cells from the subcutaneous metastasis (GI_{50} 0.001 μM) and a brain metastasis (GI_{50} 0.002 μM) grown in the presence of dabrafenib (0.15 nM to 1 μM). (C, D) PDX derived from the subcutaneous and brain lesions are both sensitive to dabrafenib when grown outside of the brain in vivo. Mice were treated with dabrafenib (25 mg/kg/day) or vehicle by oral gavage. Drug treatments commenced immediately after tumours reached 50–120 mm^3 and show individual tumour volumes (n=7–11 per group).

Notably, cells from both the baseline subcutaneous, and the dabrafenib-resistant brain lesion displayed similar sensitivity to dabrafenib in vitro (figure 2B). Similarly, patient-derived xenograft (PDX) from the two sites were equally sensitive to dabrafenib when grown in the flank of immunocompromised mice (figure 2C,D). Consistent with these results, WES of a cell line derived from the progressing brain metastasis did not reveal any mutations such as an activating mutation in *NRAS,* that could explain resistance to dabrafenib (a L25S *PIK3CA* mutation outside of the binding domain was associated with strand bias and was not confirmed by droplet digital PCR; online supplementary tables 7 and 8).

In line with other clinical responses,[2 34] the initial response of the brain lesion to dabrafenib suggested that the drug did cross the blood-brain barrier, and our data suggest that resistance was not mediated by cell-intrinsic events, so we examined if resistance was mediated by factors in the brain microenvironment. Cells were grown in serum-free medium for 24 hours in the presence or absence of dabrafenib, with or without rat CSF. Dabrafenib inhibited growth, and induced apoptosis in cells derived from the resistant tumour, but consistent with a recent report,[20] in the presence of CSF the cells overcame both the growth inhibition and induction of apoptosis mediated by dabrafenib (figure 3A,B).

Intriguingly, despite rescuing proliferation and survival, the presence of CSF did not result in reactivation of ERK in the cells from the resistant lesion (figure 3C), so we used RPPA to identify which pathways were activated. This confirmed that CSF did not reactivate MEK/ERK signalling (figure 3D,E), and also that downstream S6 phosphorylation[35] was not reactivated (figure 3F,G). However, the RPPA analysis revealed increased protein kinase B (PKB, aka AKT) phosphorylation (figure 3H,I) in the presence of CSF, suggesting that CSF induced resistance through the PI3K signalling pathway rather than alternative pathways investigated in the RPPA screen. In addition, we observed increased phosphorylation of the platelet-derived growth-factor receptor (PDGFR), which is known to activate PI3K/AKT signalling, whereas phosphorylation of other receptor tyrosine kinases was not increased (figure 3J, online supplementary table 9). We confirmed increased PI3K/AKT signalling in the presence of CSF in the cell line from the subcutaneous metastasis (online supplementary fig 3A-F), supporting an extrinsic cause for PI3K/AKT activation rather than an intrinsic cause such as a newly acquired mutation in the brain lesion cells. In addition, immunoblot showed an increase in AKT phosphorylation in the presence of CSF with and without dabrafenib (figure 3K). Accordingly, in standard media whereas dabrafenib inhibited the growth of the brain lesions cells, the PI3K/mammalian target of rapamycin (mTOR) inhibitor BEZ235 was without effect (figure 3L). Conversely, in the presence of CSF, dabrafenib no longer inhibited the growth of the brain lesion cells, whereas BEZ235 inhibited the growth of these cells (figure 3L). The switch in growth inhibition from dabrafenib to BEZ235 is consistent with rewired signalling from dependence on BRAF-ERK signalling in normal medium to dependence on PI3K signalling in CSF.

DISCUSSION

Recent studies have reported that immune therapy responses are associated with high mutation and neoantigen burden and low intratumorous heterogeneity.[36 37] Typical for acral melanoma,[8] the tumours presented here had low mutation and neoantigen burden, but despite this the patient responded to nivolumab for 12 months and was only removed from treatment due to toxicity. Our data therefore show that clinical benefit can be achieved by immune therapy in tumours that present with low mutation and neoantigen burden. This is in line with clinical studies showing that acral melanoma responses to immune therapy are similar to those of cutaneous melanoma.[5] We therefore caution against excluding patients from immune therapies solely due to low mutation burden and consequent low neoantigen load.

The patient initially mounted an impressive antitumour response on nivolumab with shrinkage of all lesions. However, resection of the progressing brain lesion following complete response provided a rare opportunity to study paired lesions, one of which escaped the immune system following checkpoint blockade. We did not find significant changes in neoantigen or MHC class I expression and did not discover mutations that would impair PTEN, IFNγ or similar signalling pathways, which can drive resistance to immune therapies.[23 25 38 39]

Notably, the brain lesion presented a gene signature and immune infiltrate associated with a significantly different microenvironment to the subcutaneous lesion. RNA-Seq data suggested increased infiltration into the brain metastasis of T regulatory cells and M2 macrophages and increased expression of genes encoding *CXCL1* and *IL10* was seen, which are associated with immunosuppression and an immunosuppressive infiltrate.[27–29] Finally, transcripts associated with checkpoints expressed on tumour infiltrating T cells such as *TIM3* and *LAG3,* which are markers of T cell exhaustion and immune therapy resistance, were increased in the brain metastasis compared with the subcutaneous lesion.[33] Critically, the brain metastasis was associated with significantly lower CD8+ effector T cell infiltration compared with the surrounding stroma, a pattern not seen in the baseline subcutaneous lesion. Decreased T cell infiltration has also been reported in cutaneous melanoma brain metastases compared with extracranial biopsy sites.[40]

Thus, immune escape did not appear to be driven by loss of the intrinsic ability of T cells to recognise and kill the tumour cells, but by the acquisition of a distinct microenvironment. This highlights the need to develop personalised medicine approaches that incorporate targeting of heterogeneous microenvironments particularly for

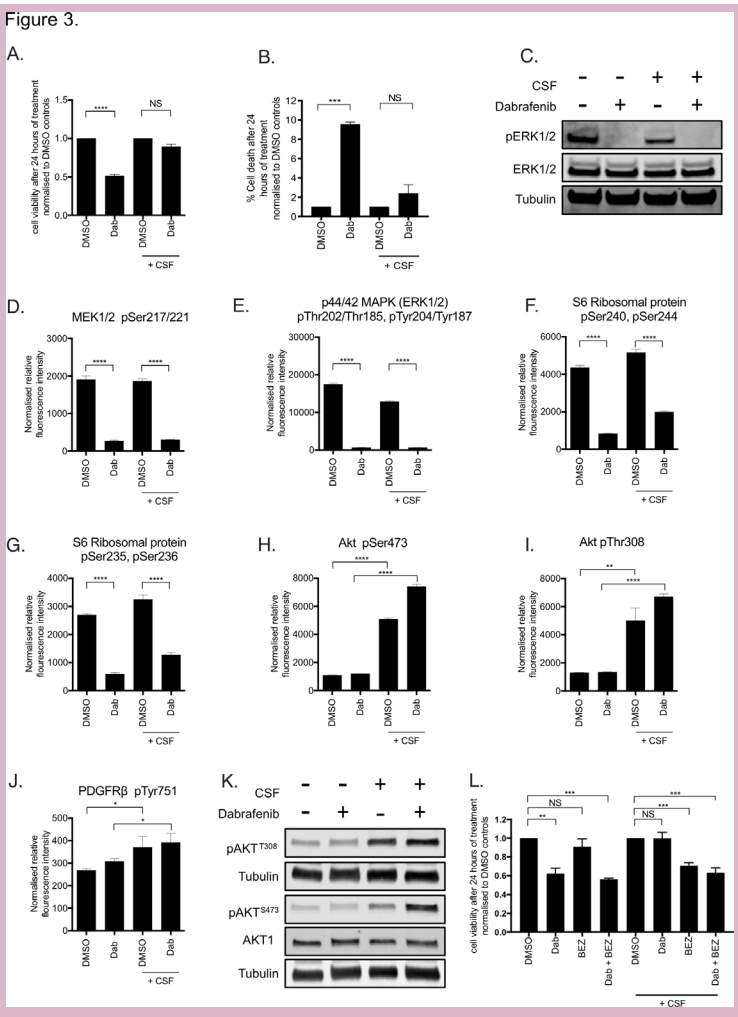

Figure 3 Cerebrospinal fluid (CSF) mediates resistance to dabrafenib through the PDGFR/PI3K/Akt pathway. (A) CSF overcomes dabrafenib-induced cell growth inhibition. Short-term growth assays showing cell growth after 24 hours following treatment with DMSO or dabrafenib (Dab; 1 µM) in RPMI or 50% CSF using CellTiter-Glo ****p<0.0001; NS, not significant. (B) CSF overcomes dabrafenib-induced cell death. Cells were cultured overnight under serum-free conditions in RPMI or 50% CSF and then treated with DMSO or dabrafenib (Dab; 1 µM) for 24 hours before assessing cell death using cleaved PARP staining measured by flow cytometry. ***p<0.001; NS, not significant. (C) CSF does not rescue MEK/ERK signalling in dabrafenib-treated cells. Cells were plated and incubated overnight in RPMI or 50% CSF under serum-free conditions before treatment of DMSO or dabrafenib 1 µM for 4 hours. Immunoblot analysis shows phosphoERK Thr$^{202/185}$ Tyr$^{204/187}$ and ERK 1/2. Tubulin was used as a loading control. (D–J) CSF rescue of cell growth correlates with PDGFR/PI3K/AKT pathway activation. Cells from the brain metastasis were incubated overnight in RPMI or 50% CSF under serum-free conditions before treatment of DMSO or dabrafenib 1 µM for 4 hours. Cell lysates were obtained and fluorescence-based nitrocellulose reverse phase protein array (RPPA) was performed for phospho-MEK1/2 (D), phospho-ERK (E), phospho-S6 (F, G), phospho-AKT (H, I), phospho-PDGFR (J), *p<0.05, **p<0.01, ****p<0.0001. (K) CSF induces AKT phosphorylation. Cells from the brain metastasis were incubated overnight in RPMI or 50% CSF under serum-free conditions before treatment of DMSO or dabrafenib 1 µM for 4 hours. Immunoblot analysis shows phospho AKT$^{T308/S473}$ and AKT1. Tubulin was used as a loading control. (L) PI3K/MTOR inhibition reduces cell growth in the presence of CSF. Graph showing cell growth measured by CellTiter-Glo 24 hours after treatment with DMSO, dabrafenib (Dab 1 µM), BEZ235 (BEZ 5 µM) or dabrafenib (Dab 1 µM) plus BEZ235 (BEZ 5 µM) in RPMI or 50% CSF under serum-free conditions. **p<0.01; ***p<0.001; NS, not significant; PDGFR, platelet-derived growth-factor receptor; PI3K, phospho-inositide 3-kinase.

patients with brain metastases or brain progression on immunotherapy.

Despite surgery and radiotherapy, the brain lesion progressed necessitating treatment with dabrafenib. Initially, the patient mounted an excellent response, and in accordance with the BREAK-MB Trial,[34] this included a shrinkage of the brain lesion. However, despite a continued extracranial response, the brain lesion relapsed rapidly. We did not find new mutations to explain resistance, and cells from the dabrafenib-resistant brain lesion remained sensitive to dabrafenib in vitro, as did the PDX derived from the pretreatment brain metastasis in the flank of immunocompromised mice. In accordance with a study by Seifert *et al*,[20] we found that CSF overcame the

antiproliferative and proapoptotic effects of dabrafenib on cells from the cranial lesion. Notably, rescue of cell growth by CSF was not accompanied by mitogen-activated protein kinase kinase - extracellular signal-regulated kinase (MEK-ERK) pathway reactivation, but by hyperactivation of the PI3K/AKT pathway. The same effect was seen in cells from the subcutaneous metastasis suggesting an extrinsic rather than intrinsic cause for the dabrafenib resistance. Unfortunately, due to the limited tissue available we were unable to confirm increased phosphorylation of protein kinase B (AKT) in the brain lesion by IHC. However, a PI3K/mTOR inhibitor significantly reduced proliferation of the cells in the presence of CSF, but had little effect on cells in media alone. This is consistent with findings from a study, which showed that a pan-PI3K inhibitor suppressed the growth of melanoma cells both in astrocyte-conditioned media and in the brains of nude mice.[41]

Thus, we show here that progression on immune and targeted therapies could be mediated by interactions between the tumour and brain microenvironment. In the case of immune therapy, immune escape was associated with a heterogeneous immune infiltrate and gene expression profile compared with the baseline lesion, whereas CSF factors contributed to resistance to targeted therapy through the PI3K/AKT pathway. The brain is a common site of treatment failure in many cancers and this site continues to be a challenge in the era of immune and targeted therapies in melanoma. However, patients with brain metastases are often excluded from clinical trials and their optimal management remains uncertain. Our study provides insight into the importance of the microenvironment in mediating resistance and we show that improved knowledge of underlying mechanisms can provide hypothesis-driven salvage treatment strategies. Thus, both mutational characteristics and the site-specific microenvironment characteristics of individual melanoma lesions need to be considered to optimise precision medicine strategies for patients with melanoma.

Author affiliations
[1]Molecular Oncology Group, CRUK Manchester Institute, The University of Manchester, Nether Alderley, UK
[2]RNA Biology Group, CRUK Manchester Institute, The University of Manchester, Nether Alderley, UK
[3]Department of Visceral, Thoracic and Vascular Surgery, German Cancer Consortium (DKTK) German Cancer Research Centre, Dresden, Germany
[4]Cancer Research UK Edinburgh Centre, Edinburgh, UK
[5]Histology Department, CRUK Manchester Institute, The University of Manchester, Nether Alderley, UK
[6]Skin Cancer and Aging Group, CRUK Manchester Institute, The University of Manchester, Nether Alderley, UK
[7]Boehringer Ingelheim International GmbH, Ingelheim, Rheinland-Pfalz, Germany
[8]Department of Medical Oncology, The Christie NHS Foundation Trust, Manchester, UK
[9]Institute of Cancer Sciences, The University of Manchester, Manchester, UK

Acknowledgements The authors thank the patient and their family for their generosity. The authors also thank the CRUK Manchester Institute core facilities with special mention to Isabel Peset, Kang Zeng, Caron Abbey, Jacqueline Swan and Lewis Woolley.The authors also thank the Christie NHS Foundation Trust and the Manchester Cancer Research Centre (MCRC) Biobank. Although the MCRC Biobank provides the samples, it cannot endorse studies conducted with, or interpretation of results from the same.

Contributors Conception and design: RJL, PL, RM. Development of methodology: RJL, GK, AM, GA, AC, CM, RM. Acquisition of data (provided animals, acquired and managed patients, provided facilities, etc): RJL, GK, FB, GA, KMC, AC, GG, EG, AM, AV, MS, PL, ND, RM. Analysis and interpretation of data (eg, statistical analysis, biostatistics, computational analysis): RJL, GK, KMC, PM, AM, CM, PL, RM. Writing, review and/or revision of the manuscript: RJL, GK, CM, ND, PL, RM. Administrative, technical or material support (ie, reporting or organising data, constructing databases): RJL, GK, NC, ND, RM. Study supervision: PL, RM.

Funding This work was supported by Cancer Research UK grant C5759/A20971 and Wellcome Trust grant 100282/Z/12/Z.

Competing interests RM Consultant Pfizer; Rewards to Inventors Scheme, Institute of Cancer Research. RJL Honoraria BMS. PL Consultant/Advisory Role: BMS, Novartis, MSD, NeraCare, Amgen, Pierre Fabre, Incyte. Honoraria: BMS, Novartis, Incyte, MSD, Amgen, NeraCare, PierreFabre. Research funding: BMS. Travel support: BMS, MSD, PierreFabre, Incyte.

Patient consent for publication Not required.

Provenance and peer review Not commissioned; externally peer reviewed.

Data availability statement All data relevant to the study are included in the article or uploaded as supplementary information. Data are available upon request.

ORCID iD
Rebecca Jane Lee http://orcid.org/0000-0003-2540-2009

REFERENCES

1 Luke JJ, Flaherty KT, Ribas A, *et al*. Targeted agents and immunotherapies: optimizing outcomes in melanoma. *Nat Rev Clin Oncol* 2017;14:463–82.
2 Davies MA, Saiag P, Robert C, *et al*. Dabrafenib plus trametinib in patients with BRAFV600-mutant melanoma brain metastases (COMBI-MB): a multicentre, multicohort, open-label, phase 2 trial. *Lancet Oncol* 2017;18:863–73.
3 Cohen JV, Tawbi H, Margolin KA, *et al*. Melanoma central nervous system metastases: current approaches, challenges, and opportunities. *Pigment Cell Melanoma Res* 2016;29:627–42.
4 Parakh S, Park JJ, Mendis S, *et al*. Efficacy of anti-PD-1 therapy in patients with melanoma brain metastases. *Br J Cancer* 2017;116:1558–63.
5 Johnson DB, Peng C, Abramson RG, *et al*. Clinical activity of ipilimumab in acral melanoma: a retrospective review. *Oncologist* 2015;20:648–52.
6 Reed R. *New concepts in surgical pathology of the skin*. John Wiley Sons, 1976: 89–90.
7 Bradford PT, Goldstein AM, McMaster ML, *et al*. Acral lentiginous melanoma: incidence and survival patterns in the United States, 1986-2005. *Arch Dermatol* 2009;145:427–34.
8 Furney SJ, Turajlic S, Stamp G, *et al*. The mutational burden of acral melanoma revealed by whole-genome sequencing and comparative analysis. *Pigment Cell Melanoma Res* 2014;27:835–8.
9 Akbani R, Akdemir KC, Aksoy BA, *et al*. Genomic classification of cutaneous melanoma. *Cell* 2015;161:1681–96.
10 Furney SJ, Pedersen M, Gentien D, *et al*. Sf3B1 mutations are associated with alternative splicing in uveal melanoma. *Cancer Discov* 2013;3:1122–9.
11 Girotti MR, Gremel G, Lee R, *et al*. Application of sequencing, liquid biopsies, and patient-derived xenografts for personalized medicine in melanoma. *Cancer Discov* 2016;6:286–99.
12 Wang K, Singh D, Zeng Z, *et al*. MapSplice: accurate mapping of RNA-Seq reads for splice junction discovery. *Nucleic Acids Res* 2010;38:e178–12.
13 Liao Y, Smyth GK, Shi W. featureCounts: an efficient General purpose program for assigning sequence reads to genomic features. *Bioinformatics* 2014;30:923–30.

14 Reimand J, Arak T, Adler P, *et al*. g:Profiler-a web server for functional interpretation of gene lists (2016 update). *Nucleic Acids Res* 2016;44:W83–9.
15 Shannon P, Markiel A, Ozier O, *et al*. Cytoscape: a software environment for integrated models of biomolecular interaction networks. *Genome Res* 2003;13:2498–504.
16 Li H, Durbin R. Fast and accurate short read alignment with Burrows-Wheeler transform. *Bioinformatics* 2009;25:1754–60.
17 McKenna A, Hanna M, Banks E, *et al*. The genome analysis toolkit: a MapReduce framework for analyzing next-generation DNA sequencing data. *Genome Res* 2010;20:1297–303.
18 Cibulskis K, Lawrence MS, Carter SL, *et al*. Sensitive detection of somatic point mutations in impure and heterogeneous cancer samples. *Nat Biotechnol* 2013;31:213–9.
19 Nielsen M, Lundegaard C, Blicher T, *et al*. NetMHCpan, a method for quantitative predictions of peptide binding to any HLA-A and -B locus protein of known sequence. *PLoS One* 2007;2:e796.
20 Seifert H, Hirata E, Gore M, *et al*. Extrinsic factors can mediate resistance to BRAF inhibition in central nervous system melanoma metastases. *Pigment Cell Melanoma Res* 2016;29:92–100.
21 Creedon H, Gómez-Cuadrado L, Tarnauskaitė Žygimantė, *et al*. Identification of novel pathways linking epithelial-to-mesenchymal transition with resistance to HER2-targeted therapy. *Oncotarget* 2016;7:11539–52.
22 Robert C, Long GV, Schachter J, *et al*. *Long-term outcomes in patients (pts) with ipilimumab (ipi)-naive advanced melanoma in the phase 3 KEYNOTE-006 study who completed pembrolizumab (pembro) treatment*. Chicago: ASCO Annual Meeting, 2017: 35. 9504.
23 Zaretsky JM, Garcia-Diaz A, Shin DS, *et al*. Mutations associated with acquired resistance to PD-1 blockade in melanoma. *N Engl J Med* 2016;375:819–29.
24 Liu C, Peng W, Xu C, *et al*. Braf inhibition increases tumor infiltration by T cells and enhances the antitumor activity of adoptive immunotherapy in mice. *Clin Cancer Res* 2013;19:393–403.
25 Dong Y, Richards J-A, Gupta R, *et al*. Pten functions as a melanoma tumor suppressor by promoting host immune response. *Oncogene* 2014;33:4632–42.
26 Spranger S, Bao R, Gajewski TF. Melanoma-intrinsic β-catenin signalling prevents anti-tumour immunity. *Nature* 2015;523:231–5.
27 Nagarsheth N, Wicha MS, Zou W. Chemokines in the cancer microenvironment and their relevance in cancer immunotherapy. *Nat Rev Immunol* 2017;17:559–72.
28 Ott PA, Hodi FS, Buchbinder EI. Inhibition of immune checkpoints and vascular endothelial growth factor as combination therapy for metastatic melanoma: an overview of rationale, preclinical evidence, and initial clinical data. *Front Oncol* 2015;5:202.
29 Tjin EPM, Krebbers G, Meijlink KJ, *et al*. Immune-Escape markers in relation to clinical outcome of advanced melanoma patients following immunotherapy. *Cancer Immunol Res* 2014;2:538–46.
30 Newman AM, Liu CL, Green MR, *et al*. Robust enumeration of cell subsets from tissue expression profiles. *Nat Methods* 2015;12:453–7.
31 Hugo W, Shi H, Sun L, *et al*. Non-Genomic and immune evolution of melanoma acquiring MAPKi resistance. *Cell* 2015;162:1271–85.
32 Kingeter LM, Lin X. C-Type lectin receptor-induced NF-κB activation in innate immune and inflammatory responses. *Cell Mol Immunol* 2012;9:105–12.
33 Anderson AC, Joller N, Kuchroo VK. Lag-3, Tim-3, and TIGIT: Co-inhibitory receptors with specialized functions in immune regulation. *Immunity* 2016;44:989–1004.
34 Long GV, Trefzer U, Davies MA, *et al*. Dabrafenib in patients with Val600Glu or Val600Lys BRAF-mutant melanoma metastatic to the brain (BREAK-MB): a multicentre, open-label, phase 2 trial. *Lancet Oncol* 2012;13:1087–95.
35 Martin MJ, Hayward R, Viros A, *et al*. Metformin accelerates the growth of BRAF ^{V600E}-driven melanoma by upregulating VEGF-A. *Cancer Discov* 2012;2:344–55.
36 Snyder A, Makarov V, Merghoub T, *et al*. Genetic basis for clinical response to CTLA-4 blockade in melanoma. *N Engl J Med* 2014;371:2189–99.
37 McGranahan N, Furness AJS, Rosenthal R, *et al*. Clonal neoantigens elicit T cell immunoreactivity and sensitivity to immune checkpoint blockade. *Science* 2016;351:1463–9.
38 Verdegaal EME, de Miranda NFCC, Visser M, *et al*. Neoantigen landscape dynamics during human melanoma-T cell interactions. *Nature* 2016;536:91–5.
39 Peng W, Chen JQ, Liu C, *et al*. Loss of PTEN promotes resistance to T cell-mediated immunotherapy. *Cancer Discov* 2016;6:202–16.
40 Fischer GM, Jalali A, Kircher DA, *et al*. Molecular profiling reveals unique immune and metabolic features of melanoma brain metastases. *Cancer Discov* 2019;9:628–45.
41 Niessner H, Schmitz J, Tabatabai G, *et al*. Pi3K pathway inhibition achieves potent antitumor activity in melanoma brain metastases in vitro and in vivo. *Clin Cancer Res* 2016;22:5818–28.